
Certifying Model Accuracy under Distribution Shifts

Aounon Kumar¹ Alexander Levine¹ Tom Goldstein¹ Soheil Feizi¹

Abstract

Certified robustness in machine learning has primarily focused on adversarial perturbations of the input with a fixed attack budget for each point in the data distribution. In this work, we present provable robustness guarantees on the accuracy of a model under bounded Wasserstein shifts of the data distribution. We show that a simple procedure that randomizes the input of the model within a transformation space is provably robust to distributional shifts under the transformation. Our framework allows the datum-specific perturbation size to vary across different points in the input distribution and is general enough to include fixed-sized perturbations as well. Our certificates produce guaranteed lower bounds on the performance of the model for any (natural or adversarial) shift of the input distribution within a Wasserstein ball around the original distribution. We apply our technique to: (i) certify robustness against natural (non-adversarial) transformations of images such as color shifts, hue shifts and changes in brightness and saturation, (ii) certify robustness against adversarial shifts of the input distribution, and (iii) show provable lower bounds (hardness results) on the performance of models trained on so-called “unlearnable” datasets that have been poisoned to interfere with model training.

1. Introduction

Machine learning models often suffer significant performance loss under minor shifts in the data distribution that do not affect a human’s ability to perform the same task— e.g., input noise (Dodge & Karam, 2016; Geirhos et al., 2018), image scaling, shifting and translation (Azulay & Weiss, 2019), spatial (Engstrom et al., 2019) and geometric transformations (Fawzi & Frossard, 2015; Alcorn et al., 2019), blurring (Vasiljevic et al., 2016; Zhou et al., 2017), acoustic

corruptions (Pearce & Hirsch, 2000) and adversarial perturbations (Szegedy et al., 2014; Carlini & Wagner, 2017; Goodfellow et al., 2015; Madry et al., 2018; Biggio et al., 2013). Overcoming such robustness challenges is a major hurdle for deploying these models in real-world safety-critical applications where reliability of the predictions made is paramount. Several training techniques have been developed to improve the empirical robustness of models to data shifts, e.g., diversifying datasets (Taori et al., 2020), training with natural corruptions (Hendrycks & Dietterich, 2019), data augmentations (Yang et al., 2019), contrastive learning (Kim et al., 2020; Radford et al., 2021; Ge et al., 2021) and adversarial training (Goodfellow et al., 2015; Madry et al., 2018; Tramèr & Boneh, 2019; Shafahi et al., 2019; Maini et al., 2020). These methods are designed to withstand specific ways of introducing changes in inputs (e.g., a particular adversarial attack procedure) and may break down under a different method for generating perturbations, e.g., adversarial defenses becoming ineffective under newer attacks (Carlini & Wagner, 2017; Athalye et al., 2018; Uesato et al., 2018; Laidlaw & Feizi, 2019; Laidlaw et al., 2021).

Certifiable robustness, on the other hand, seeks to produce provable guarantees on the adversarial robustness of a model which hold regardless of the attack strategy. However, the study of provable robustness has mostly focused on perturbations with a fixed size budget (e.g., an ℓ_p -ball of same size) for all input points (Cohen et al., 2019; Lécuyer et al., 2019; Li et al., 2019; Salman et al., 2019; Goyal et al., 2018; Huang et al., 2019; Wong & Kolter, 2018; Raghu-nathan et al., 2018; Singla & Feizi, 2019; 2020; Levine & Feizi, 2021; 2020a;b). Among provable robustness methods, randomized smoothing based procedures have been able to successfully scale up to high-dimensional problems (Cohen et al., 2019; Lécuyer et al., 2019; Li et al., 2019; Salman et al., 2019) and adapted effectively to other domains such as reinforcement learning (Kumar et al., 2021; Wu et al., 2021) and models with structured outputs (Kumar & Goldstein, 2021). Existing techniques do not extend to the aforementioned data shifts as the perturbations for each input point in the distribution need not have a fixed bound on their size. For example, stochastic changes in the input images of a vision model caused by lighting and weather conditions may vary across time and location. Even adversarial attacks may adjust the perturbation size depending on the input instance.

¹Department of Computer Science, University of Maryland, USA. Correspondence to: Aounon Kumar <aounon@umd.edu>, Soheil Feizi <sfeizi@cs.umd.edu>.

Robustness against natural as well as adversarial shifts in the distribution is a major challenge for deploying machine learning algorithms in safety-critical applications such as self-driving, medical diagnosis and critical infrastructure. Verifiable robustness to both these shifts is an important goal in designing reliable real-world systems. A standard way to describe such data shifts is to constrain the Wasserstein distance between the original distribution \mathcal{D} and the shifted distribution $\tilde{\mathcal{D}}$, i.e., $W_1^d(\mathcal{D}, \tilde{\mathcal{D}}) \leq \epsilon$, for an appropriate distance function d over the input space and a real number ϵ . It essentially bounds the average perturbation size across the entire distribution instead of putting a hard budget constraint for each input point. Wasserstein distance is a standard similarity measure for probability distributions and has been extensively used to study distribution shifts (Courty et al., 2017; Damodaran et al., 2018; Lee & Raginsky, 2018; Wu et al., 2019). Certifiable robustness against Wasserstein shifts is an interesting problem to study in its own right and a useful tool to have in the arsenal of provable robustness techniques in machine learning.

In this work, we present an efficient procedure to make any model robust to distributional shifts with verifiable guarantees on its performance. We consider families of parameterized distribution shifts which may include shifts in the RGB color balance of an image, the hue/saturation balance, the brightness/contrast, and more. To achieve distributional robustness, we randomize the input to our model by replacing each input image with a shifted image randomly sampled from a smoothing distribution. By randomizing in this way, a given model can be made provably robust to any shifted distribution (natural or adversarial) within a Wasserstein radius ϵ from the original distribution.

We design robustness certificates that bound the difference between the accuracy of the robust model under the distributions \mathcal{D} and $\tilde{\mathcal{D}}$ as a function of ϵ . For a function \bar{h} representing the performance of the robust model, our main theoretical result in Theorem 4.1 shows that

$$|\mathbb{E}_{x \sim \mathcal{D}}[\bar{h}(x)] - \mathbb{E}_{z \sim \tilde{\mathcal{D}}}[\bar{h}(z)]| \leq \psi(\epsilon),$$

where $\psi(\epsilon)$ is a concave function satisfying condition (2) in Section 3. This result places a Lipschitz-like bound on the change in performance with respect to the Wasserstein distance of the shifted distribution.

Robustness under distribution shifts is a fundamental problem in several areas of machine learning and our certificates could be applicable to a multitude of learning tasks. Our method does not make any assumptions on the model or significantly increase its computational requirements as it only needs one sample per input to make robust predictions, making it viable for real-world applications using conventional neural network architectures. The sample complexity for generating Wasserstein certificates over the entire distri-

bution is roughly the same as obtaining adversarial certificates for a single input instance using existing randomized smoothing based techniques (Cohen et al., 2019; Salman et al., 2019). We demonstrate the usefulness of our main theoretical result (Theorem 4.1) in three domains:

(i) Certifying model accuracy under natural shifts of the data distribution (Section 5):

We consider three image transformations: color shift, hue shift and changes in brightness and saturation (SV shift). We define a parameter space for each of these transformations in such a way that the transformations satisfy properties, such as additive composability (equation (4)), required for the certificates. We show that by randomizing the input of a model in the parameter space of the transformation, we can derive distribution level robustness certificates which guarantee that the accuracy of the model will remain above a threshold for any shifted distribution within an ϵ -sized Wasserstein ball around the original input distribution. Figure (1) visualizes CIFAR-10 images under each of these transformations and reports the corresponding certified accuracies obtained by our method. Figure (2) plots the accuracy of two base models (trained on CIFAR-10 images with and without noise in the transformation space) under a shifted distribution and compares it with the certified accuracy of a robust model (noise-trained model smoothed using input randomization). These results demonstrate that our certificates are significant and non-vacuous (see appendix E for more details).

(ii) Certifying population level robustness against adversarial attacks (Section 6):

The distribution of instances generated by an adversarial attack can also be viewed as a shift in the input distribution within a Wasserstein bound. The Wasserstein distance of such a shift is given by the average size of the perturbation (ℓ_2 -norm) added per input instance in the data distribution. Since our certificates work for any distribution shift (natural or adversarial) satisfying the Wasserstein bound, we can certify the accuracy of models against adversarial attacks as well. Unlike existing certification techniques which assume a fixed perturbation budget across all inputs (Cohen et al., 2019; Lécuyer et al., 2019; Li et al., 2019; Salman et al., 2019), our guarantees work for a more general threat model where the adversary is allowed to choose the perturbation size for each input instance as long as it respects the constraint on the average perturbation size over the entire data distribution. Also, our procedure only requires *one* sample from the smoothing distribution per input instance which makes computing population level certificates significantly more efficient than existing techniques. The certified accuracy we obtain significantly outperforms the base model under attack (figure 5).

(iii) Hardness results for generating “unlearnable” datasets (Section 7):

(Huang et al., 2021) proposed a method to make regular datasets unusable for modern deep learning models by poisoning them with adversarial per-

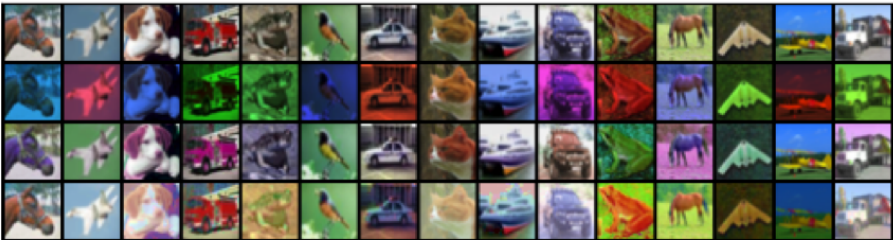

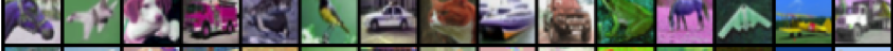

		Wasserstein Distance	Certified Accuracy
Original		-	-
Color Shift		0.5	78.5%
Hue Shift		90°	87.6%
SV Shift		1.0	59.8%

Figure 1. Certified accuracies obtained for different natural transformations of CIFAR-10 images such as color shifts, hue shifts and changes in brightness and saturation. The Wasserstein distance of each distribution shift from the original distribution is defined with respect to the corresponding distance function.

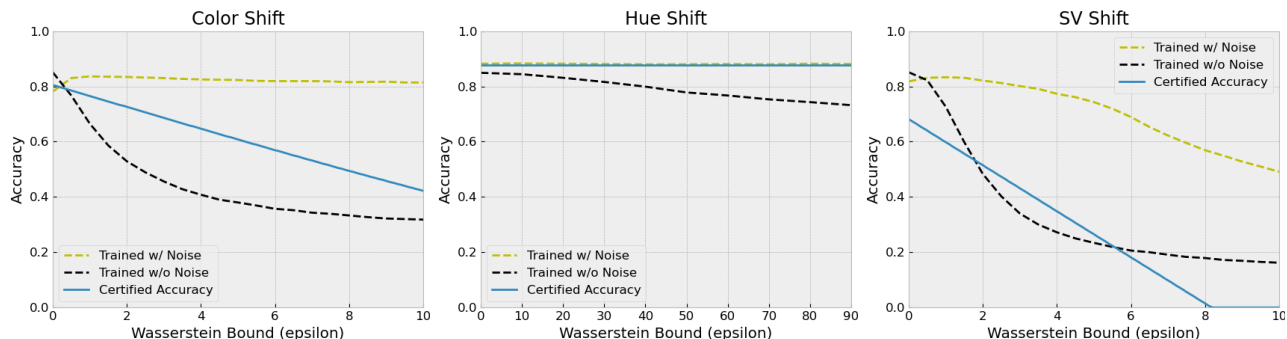


Figure 2. Comparison between the empirical performance (dashed lines) of two base models (trained on CIFAR-10 images with and without noise in transformation space) and the certified accuracy (solid line) of a robust model (noise-trained model smoothed using input randomization) under distribution shifts. The certified accuracy (against worst-case shifts) often outperforms the undefended model and remains reasonably close (almost overlaps for hue shift) to the model trained under noise for small shifts in the distribution.

turbations to interfere with the training of the model. The intended purpose is to increase privacy for sensitive data such as personal images uploaded to social media sites. The dataset is poisoned in such a way that a model that minimizes the loss on this data distribution will have low accuracy on clean test samples. We show that our framework can obtain verifiable lower bounds on the performance of a model trained on such unlearnable datasets. Our certificates guarantee that the performance of the robust model (using input randomization) will remain above a certain threshold on the test distribution even when the base model is trained on the poisoned dataset with a smoothing noise of suitable magnitude. This demonstrates a fundamental limitation in producing unlearnable datasets.

2. Related Work

Augmenting training data with corruptions has been shown to improve empirical robustness of machine learning models (Hendrycks & Dietterich, 2019; Yang et al., 2019; Goodfellow et al., 2015; Madry et al., 2018). Training a model with randomly transformed inputs, such as blurring, cropping and rotating images, can improve its test performance against such perturbations. However, these methods do not seek to produce guarantees on the performance of the model

with respect to the extent of the shift in the data distribution. Our method applies transformations during inference to produce verifiable performance guarantees against any shift in the data distribution within the certified Wasserstein radius. It does not depend on the underlying model’s architecture or the training procedure and may be coupled with robust training techniques to improve the certified guarantees.

Smoothing based approaches that aggregate the predictions on a large number of noisy samples of the input (Cohen et al., 2019; Lécuyer et al., 2019; Li et al., 2019; Salman et al., 2019) and that use input randomization (Pinot et al., 2021) have been studied in the context of certified adversarial robustness. Certified robustness for parameterized transformations on images also exist (Fischer et al., 2020). These techniques produce instance-wise certificates and do not generate guarantees on shifts in the data distribution with varying perturbation budget across different points in the distribution. Our work also differs from instance-wise adversarial attacks and defenses (Wong et al., 2019; Levine & Feizi, 2019) that use the Wasserstein distance (instead of conventional ℓ_p distances) to measure difference between an image and its perturbed counterpart. In contrast, our certificates consider the Wasserstein distance between data distributions from which images themselves are sampled.

(Sinha et al., 2018) studied robustness to distribution shifts in the context of adversarial attacks and obtained guarantees on the population loss on MNIST and synthetic datasets. They model these shifts using the Wasserstein metric for ℓ_2 distance and bound the population loss using a Lagrangian relaxation of the robust optimization problem. Their bound requires a Lipschitz constant for the neural network model, which becomes extremely large and intractable for deep networks. Our certificates do not make any assumptions on the base model. Additionally, our approach can certify the model’s accuracy under non- ℓ_p changes to the input images, such as visible color shifts, for which the ℓ_2 -norm of the perturbation in the image space will be very high.

3. Preliminaries and Notations

Let \mathcal{D} and $\tilde{\mathcal{D}}$ denote the original and shifted distributions respectively over an input space \mathcal{X} such that the Wasserstein distance, with respect to a given distance function $d : \mathcal{X} \times \mathcal{X} \rightarrow \mathbb{R}_{\geq 0}$, between the two distributions is bounded by ϵ (i.e., $W_1^d(\mathcal{D}, \tilde{\mathcal{D}}) \leq \epsilon$). This implies that there exists an element γ^* in the set $\Gamma(\mathcal{D}, \tilde{\mathcal{D}})$ of all joint distributions with marginals $\mu_{\mathcal{D}}$ and $\mu_{\tilde{\mathcal{D}}}$ such that

$$\int_{\mathcal{X}} \int_{\mathcal{X}} d(x, z) \gamma^*(x, z) dx dz \leq \epsilon. \quad (1)$$

Let $\mathcal{S} : \mathcal{X} \rightarrow \Delta(\mathcal{X})$ be a function mapping each element $x \in \mathcal{X}$ to a smoothing distribution $\mathcal{S}(x) \in \Delta(\mathcal{X})$, where $\Delta(\mathcal{X})$ is the set of all probability distributions over \mathcal{X} . For example, smoothing with an isometric Gaussian noise distribution with variance σ^2 can be denoted as $\mathcal{S}(x) = \mathcal{N}(x, \sigma^2 I)$. Let the total variation between the smoothing distributions at two points x and z be bounded by a concave increasing function ψ of the distance between them, i.e.,

$$\text{TV}(\mathcal{S}(x), \mathcal{S}(z)) \leq \psi(d(x, z)). \quad (2)$$

For example, when the distance function d is the ℓ_2 -norm of the difference of x and z , and the smoothing distribution is an isometric Gaussian $\mathcal{N}(0, \sigma^2 I)$ with variance σ^2 , $\psi(\cdot) = \text{erf}(\cdot/2\sqrt{2}\sigma)$ is a valid upper bound on the above total variation that is concave in the positive domain (see appendix B for more examples).

Consider a function $h : \mathcal{X} \rightarrow [0, 1]$ that represents the accuracy of a model. For example, in the case of a classifier $\mu : \mathcal{X} \rightarrow \mathcal{Y}$ that maps inputs from space \mathcal{X} to a class label in \mathcal{Y} , $h(x) := \mathbf{1}\{\mu(x) = \text{GT}(x)\}$ could be the indicator function for when the prediction of the model $\mu(x)$ matches the ground truth label $\text{GT}(x)$. The overall accuracy of the model μ is then given by $\mathbb{E}_{x \in \mathcal{D}}[h(x)]$. Our goal is to bound the difference in the expected performance of a model between the original distribution \mathcal{D} and the shifted distribution

$\tilde{\mathcal{D}}$. Using a smoothing distribution \mathcal{S} , define a *smoothed* version of the function h as below:

$$\bar{h}(x) = \mathbb{E}_{x' \sim \mathcal{S}(x)}[h(x')]. \quad (3)$$

Our main theoretical result (Theorem 4.1) bounds the difference between the expected value of \bar{h} under \mathcal{D} and $\tilde{\mathcal{D}}$ using the function ψ and the Wasserstein bound ϵ .

3.1. Parameterized Transformations

We apply our distributional robustness certificates to certify the accuracy of an image classifier under natural transformations of the images such as color shifts, hue shifts and changes in brightness and saturation. We model each of them as a parameterized transformation $\mathcal{T} : \mathcal{X} \times P \rightarrow \mathcal{X}$ which is a function over the input/image space \mathcal{X} and a parameter space P which takes an image $x \in \mathcal{X}$ and a parameter vector $\theta \in P$ and outputs a transformed image $x' = \mathcal{T}(x, \theta) \in \mathcal{X}$. An example of such a transformation could be a color shift in an RGB image produced by scaling the intensities in the red, green and blue channels $x = (\{x_{ij}^R\}, \{x_{ij}^G\}, \{x_{ij}^B\})$ defined as $\text{CS}(x, \theta) = (2^{\theta_R} \{x_{ij}^R\}, 2^{\theta_G} \{x_{ij}^G\}, 2^{\theta_B} \{x_{ij}^B\}) / \text{MAX}$ for a tuple $\theta = (\theta_R, \theta_G, \theta_B)$, where MAX is the maximum of all the RGB values after scaling. Another example could be vector translations $\text{VT}(x, \theta) = x + \theta$. In order to apply randomized smoothing, we assume that the transformation returns x if the parameters are all zero, i.e., $\mathcal{T}(x, 0) = x$ and that the composition of two transformations with parameters θ_1 and θ_2 is a transformation with parameters $\theta_1 + \theta_2$ (additive composability), i.e.,

$$\mathcal{T}(\mathcal{T}(x, \theta_1), \theta_2) = \mathcal{T}(x, \theta_1 + \theta_2). \quad (4)$$

Given a norm $\|\cdot\|$ in the parameter space P , we define a distance function in the input space \mathcal{X} as follows:

$$d_{\mathcal{T}}(x_1, x_2) = \begin{cases} \min\{\|\theta\| & \text{s.t. } \mathcal{T}(x_1, \theta) = x_2\} \\ \infty & \text{otherwise.} \end{cases} \quad (5)$$

Now, define a smoothing distribution $\mathcal{S}(x) = \mathcal{T}(x, \mathcal{Q}(0))$ for some distribution \mathcal{Q} in the parameter space of \mathcal{T} such that $\forall \theta \in P, \mathcal{Q}(\theta) = \theta + \mathcal{Q}(0)$ is the distribution of $\theta + \delta$ where $\delta \sim \mathcal{Q}(0)$, and $\text{TV}(\mathcal{Q}(0), \mathcal{Q}(\theta)) \leq \psi(\|\theta\|)$ for a concave function ψ . For example, $\mathcal{Q}(\cdot) = \mathcal{N}(\cdot, \sigma^2 I)$ satisfies these properties for $\psi(\cdot) = \text{erf}(\cdot/2\sqrt{2}\sigma)$. Then, the following lemma holds (proof in appendix A):

Lemma 3.1. *For two points $x, z \in \mathcal{X}$ such that $d_{\mathcal{T}}(x, z)$ is finite,*

$$\text{TV}(\mathcal{S}(x), \mathcal{S}(z)) \leq \psi(d_{\mathcal{T}}(x, z)).$$

4. Certified Distributional Robustness

In this section, we prove our main theoretical result showing that the difference in the expectation of the smoothed function \bar{h} defined in equation (3) under the original distribution \mathcal{D} and the shifted distribution $\tilde{\mathcal{D}}$ can be bounded by the Wasserstein distance between \mathcal{D} and $\tilde{\mathcal{D}}$. Given a concave upper bound ψ on the total variation between the smoothing distributions at two points x and z (i.e., satisfying condition (2)), the following theorem holds.

Theorem 4.1. *Given a function $h : \mathcal{X} \rightarrow [0, 1]$, define its smoothed version as $\bar{h}(x) = \mathbb{E}_{x' \sim \mathcal{S}(x)}[h(x')]$. Then,*

$$|\mathbb{E}_{x \sim \mathcal{D}}[\bar{h}(x)] - \mathbb{E}_{z \sim \tilde{\mathcal{D}}}[\bar{h}(z)]| \leq \psi(\epsilon).$$

Proof. For any joint distribution $\gamma \in \Gamma(\mathcal{D}, \tilde{\mathcal{D}})$ we have

$$\begin{aligned} \mathbb{E}_{x \sim \mathcal{D}}[\bar{h}(x)] &= \int_{\mathcal{X}} \bar{h}(x) \mu_{\mathcal{D}}(x) dx \\ &= \int_{\mathcal{X}} \bar{h}(x) \left(\int_{\mathcal{X}} \gamma(x, z) dz \right) dx \\ &\quad \text{(definition of } \Gamma) \\ &= \int_{\mathcal{X}} \int_{\mathcal{X}} \bar{h}(x) \gamma(x, z) dz dx \\ &= \int_{\mathcal{X}} \int_{\mathcal{X}} \bar{h}(x) \gamma(x, z) dx dz. \end{aligned}$$

Similarly,

$$\begin{aligned} \mathbb{E}_{z \sim \tilde{\mathcal{D}}}[\bar{h}(z)] &= \int_{\mathcal{X}} \bar{h}(z) \mu_{\tilde{\mathcal{D}}}(z) dz \\ &= \int_{\mathcal{X}} \bar{h}(z) \left(\int_{\mathcal{X}} \gamma(x, z) dx \right) dz \\ &\quad \text{(definition of } \Gamma) \\ &= \int_{\mathcal{X}} \int_{\mathcal{X}} \bar{h}(z) \gamma(x, z) dx dz. \end{aligned}$$

Therefore,

$$\begin{aligned} &|\mathbb{E}_{x \sim \mathcal{D}}[\bar{h}(x)] - \mathbb{E}_{z \sim \tilde{\mathcal{D}}}[\bar{h}(z)]| \\ &= \left| \int_{\mathcal{X}} \int_{\mathcal{X}} \bar{h}(x) \gamma(x, z) dx dz - \int_{\mathcal{X}} \int_{\mathcal{X}} \bar{h}(z) \gamma(x, z) dx dz \right| \\ &\leq \int_{\mathcal{X}} \int_{\mathcal{X}} |\bar{h}(x) - \bar{h}(z)| \gamma(x, z) dx dz \\ &\leq \int_{\mathcal{X}} \int_{\mathcal{X}} \text{TV}(\mathcal{S}(x), \mathcal{S}(z)) \gamma(x, z) dx dz \\ &\leq \int_{\mathcal{X}} \int_{\mathcal{X}} \psi(d(x, z)) \gamma(x, z) dx dz \quad \text{(from condition (2))} \\ &\leq \psi \left(\int_{\mathcal{X}} \int_{\mathcal{X}} d(x, z) \gamma(x, z) dx dz \right). \\ &\quad (\psi \text{ is concave and Jensen's inequality}) \end{aligned}$$

Since $\gamma^* \in \Gamma(\mathcal{D}, \tilde{\mathcal{D}})$, we have:

$$\begin{aligned} &|\mathbb{E}_{x \sim \mathcal{D}}[\bar{h}(x)] - \mathbb{E}_{z \sim \tilde{\mathcal{D}}}[\bar{h}(z)]| \\ &\leq \psi \left(\int_{\mathcal{X}} \int_{\mathcal{X}} d(x, z) \gamma^*(x, z) dx dz \right) \\ &\leq \psi(\epsilon). \quad \text{(from bound (1))} \end{aligned}$$

□

In the above proof, we first express $\mathbb{E}_{x \sim \mathcal{D}}[\bar{h}(x)]$ and $\mathbb{E}_{z \sim \tilde{\mathcal{D}}}[\bar{h}(z)]$ as an expectation over a joint distribution $\gamma \in \Gamma(\mathcal{D}, \tilde{\mathcal{D}})$ with marginals $\mu_{\mathcal{D}}$ and $\mu_{\tilde{\mathcal{D}}}$. Then, we show that for any such γ , the difference in the expectations can be bounded by ψ of the expected distance under γ . Since the optimal joint distribution γ^* from condition (1) is also an element of $\Gamma(\mathcal{D}, \tilde{\mathcal{D}})$, the difference is bounded by $\psi(\epsilon)$. The intuition behind this guarantee is that if the overlap between the smoothing distributions between two individual points does not decrease rapidly with the distance between them (i.e., can be lower bounded), then the overlap between the original and the shifted distributions remains high when the Wasserstein distance between them is small.

Thus, for a shift within a Wasserstein bound of ϵ , the accuracy of the model can be bounded as $\mathbb{E}_{z \sim \tilde{\mathcal{D}}}[\bar{h}(z)] \geq \mathbb{E}_{x \sim \mathcal{D}}[\bar{h}(x)] - \psi(\epsilon)$. But, in practice, we may only estimate $\mathbb{E}_{x \sim \mathcal{D}}[\bar{h}(x)]$ using a finite number of samples. In our experiments, we compute a confidence lower bound using the Clopper-Pearson method that holds with $1 - \alpha$ probability (for some $\alpha > 0$, usually 0.001) on the robust model's accuracy on the original distribution (Clopper & Pearson, 1934). In the following sections, we will demonstrate the usefulness of this fundamental result in several applications.

5. Certified Accuracy against Natural Transformations

We certify the accuracy of a ResNet-110 model trained on CIFAR-10 images under three types of image transformations: color shifts, hue shifts and variation in brightness and saturation (SV shift). We train our models with varying levels of noise in the transformation space and evaluate their certified performance using smoothing distributions of different noise levels. For color and SV shifts, we show how the certified accuracy as a function of the Wasserstein distance varies as we change the training and smoothing noise. For hue shift, we use a smoothing distribution (with fixed noise level) that is invariant to rotations in hue space and the certified accuracy remains constant with respect to the corresponding Wasserstein distance. Training each model for 90 epochs takes a few hours on a single NVIDIA GeForce RTX 2080 Ti GPU and computing the distribution level Wasserstein certificates using 10^5 samples with 99.9% confidence takes about 25 seconds.

Certifying Model Accuracy under Distribution Shifts

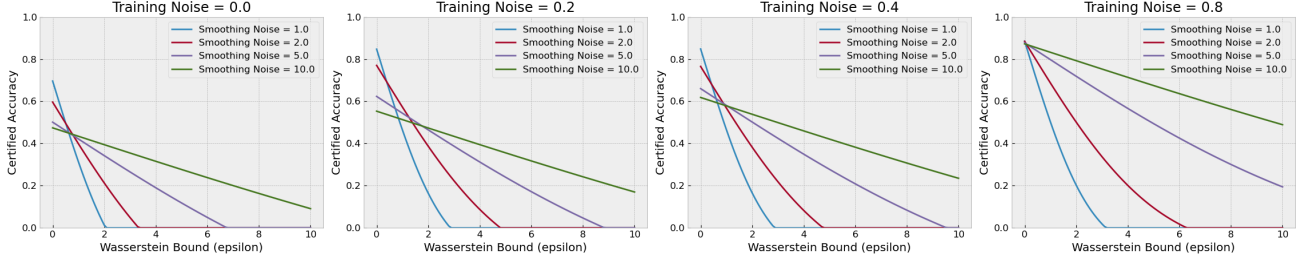


Figure 3. Certified accuracy under color shifts. Each plot corresponds to a particular training noise and each curve corresponds to a particular smoothing noise.

5.1. Color Shifts

Denote an RGB image x as an $H \times W$ array of pixels where the red, green and blue components of the pixel in the i th row and j th column are given by the tuple $x_{ij} = (r, g, b)_{ij}$. Let r_{\max}, g_{\max} and b_{\max} be the maximum values of the red, green and blue channels, respectively. Assume that the RGB values are in the interval $[0, 1]$ normalized such that the maximum over all intensity values is one, i.e., $\max(r_{\max}, g_{\max}, b_{\max}) = 1$. Define a color shift of the image x for a parameter vector $\theta \in \mathbb{R}^3$ as

$$\text{CS}(x, \theta) = \left\{ \frac{(2^{\theta_R} r, 2^{\theta_G} g, 2^{\theta_B} b)_{ij}}{\max(2^{\theta_R} r_{\max}, 2^{\theta_G} g_{\max}, 2^{\theta_B} b_{\max})} \right\}^{H \times W}$$

which scales the intensities of each channel by the corresponding component of θ raised to the power of two and then normalizes the scaled image so that the maximum intensity is one. For example, $\theta = (1, -1, 0)$ would first double all the red intensities, halve the green intensities and leave the blue intensities unchanged, and then, normalize the image so that the maximum intensity value over all the channels is equal to one.

Theorem 5.1. *The transformation CS satisfies the additive composability property, i.e., $\forall x \in M, \theta_1, \theta_2 \in \mathbb{R}^3$,*

$$\text{CS}(\text{CS}(x, \theta_1), \theta_2) = \text{CS}(x, \theta_1 + \theta_2).$$

Given an image x , we define a smoothing distribution around x in the parameter space as $\text{CS}(x, \delta)$ where $\delta \sim \mathcal{N}(0, \sigma^2 I_{3 \times 3})$. Define the distance function d_{CS} as described in (5) using the ℓ_2 -norm in the parameter space. For a distribution $\tilde{\mathcal{D}}$ within a Wasserstein distance of ϵ , under the distance function d_{CS} , from the original distribution \mathcal{D} , the performance of the smoothed model on $\tilde{\mathcal{D}}$ can be bounded as

$$\mathbb{E}_{z \sim \tilde{\mathcal{D}}}[\bar{h}(z)] \geq \mathbb{E}_{x \sim \mathcal{D}}[\bar{h}(x)] - \text{erf}(\epsilon/2\sqrt{2}\sigma).$$

Figure 3 plots the certified accuracy under color shift with respect to the Wasserstein bound ϵ for different values of training and smoothing noise. In appendix G, we consider a

smoothing distribution that randomly picks one color channel achieving a constant certified accuracy of 87.1% with respect to the Wasserstein bound ϵ .

5.2. Hue Shift

Any RGB image can be alternatively represented in the HSV image format by mapping the (r, g, b) tuple for each pixel to a point (h, s, v) in a cylindrical coordinate system where the values h, s and v represent the hue, saturation and brightness (value) of the pixel. The mapping from the RGB coordinate to the HSV coordinate takes the $[0, 1]^3$ color cube and transforms it into a cylinder of unit radius and height. The hue values are represented as angles in $[0, 2\pi)$ and the saturation and brightness values are in $[0, 1]$. Define a hue shift of an $H \times W$ sized image x by an angle $\theta \in [-\pi, \pi]$ in the HSV space as:

$$\text{HS}(x, \theta) = \left\{ (w(h + \theta), s, v)_{ij} \right\}^{H \times W}$$

where $w(x) = x - 2\pi \left\lfloor \frac{x}{2\pi} \right\rfloor$

which rotates each hue value by an angle θ and wraps it around to the $[0, 2\pi)$ range. It is easy to show that this transformation satisfies the desired properties in Section 3.1 such as additive composability. The Wasserstein distance is defined using the corresponding distance function d_{HS} by taking the absolute value of the hue shift $|\theta|$.

Define a smoothing distribution that applies a random hue rotation δ sampled uniformly from the range $[-\pi, \pi]$. Since HS wraps the hue values around in the interval, the distributions of $h + \delta$ and $(h + \theta) + \delta$ for two hue values shifted by an angle θ are both uniform in $[0, 2\pi]$. Thus, the smoothing distribution for two hue shifted images is the same which implies that $\psi(d(x, z)) = 0$ whenever $d(x, z)$ is finite. Hence, from Theorem 4.1, we have $\mathbb{E}_{z \sim \tilde{\mathcal{D}}}[\bar{h}(z)] \geq \mathbb{E}_{x \sim \mathcal{D}}[\bar{h}(x)]$ for hue shifts. Since, the certified accuracy remains constant with respect to the Wasserstein distance of the shift, we plot the certified accuracies obtained by various base models trained using different noise level in appendix F.

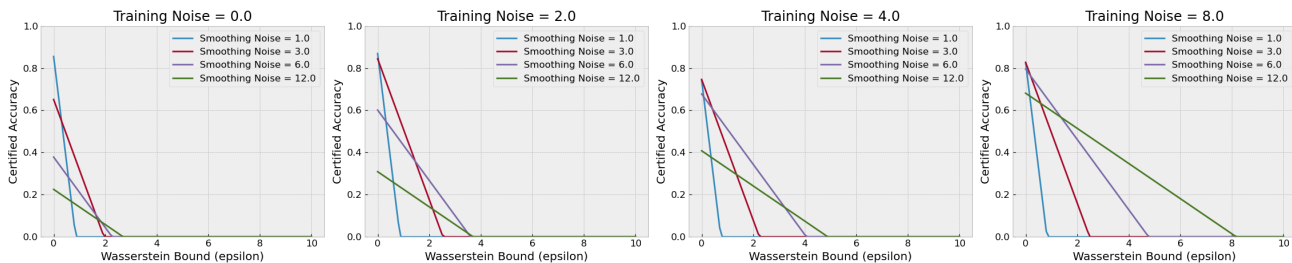


Figure 4. Certified accuracy under brightness and saturation changes. Each plot corresponds to a particular training noise and each curve corresponds to a particular smoothing noise.

5.3. Brightness and Saturation Changes

Define the following transformation in the HSV space of an image that shifts the mean of the saturation (S) and brightness (V) values for each pixel by a certain amount:

$$SV(x, \theta) = \left\{ \left(h, \frac{s + (2^{\theta_s} - 1)s_{\text{mean}}}{\text{MAX}}, \frac{v + (2^{\theta_v} - 1)v_{\text{mean}}}{\text{MAX}} \right)_{ij} \right\}^{H \times W}$$

where $s_{\text{mean}}, s_{\text{max}}, v_{\text{mean}}$ and v_{max} are the means and maximums of the saturation and brightness values respectively before the shift is applied and $\text{MAX} = \max(s_{\text{max}} + (2^{\theta_s} - 1)s_{\text{mean}}, v_{\text{max}} + (2^{\theta_v} - 1)v_{\text{mean}})$ is the maximum of the brightness and saturation values after the shift.

Theorem 5.2. *The transformation SV satisfies the additive composability property, i.e., $\forall x \in M, \theta_1, \theta_2 \in \mathbb{R}_{\geq 0}^2$,*

$$SV(SV(x, \theta_1), \theta_2) = SV(x, \theta_1 + \theta_2).$$

Figure 4 plots the certified accuracy under saturation and brightness changes with respect to the Wasserstein bound ϵ for different values of training and smoothing noise. The smoothing distribution for this transformation is a uniform in the range $[0, a]^2$ in the parameter space, the distance function is the ℓ_1 -norm and $\psi(\epsilon) = \min(\epsilon/a, 1)$.

6. Population-Level Certificates against Adversarial Attacks

Here, rather than parameterized transformations, we consider distributional shifts where the input-space distance function $d(x, z)$ which defines the Wasserstein metric is the pixel-space ℓ_2 distance. We can then use a pixel-space Gaussian smoothing distribution: $\mathcal{S}(x) = \mathcal{N}(x, \sigma^2 I)$.

To motivate this, consider an attacker function $\text{Adv} \in \mathcal{X} \rightarrow \mathcal{X}$, which takes an image x and computes $\text{Adv}(x)$, an adversarially-perturbed version of x which may have features that make it likely to be misclassified. If $x \sim \mathcal{D}$,

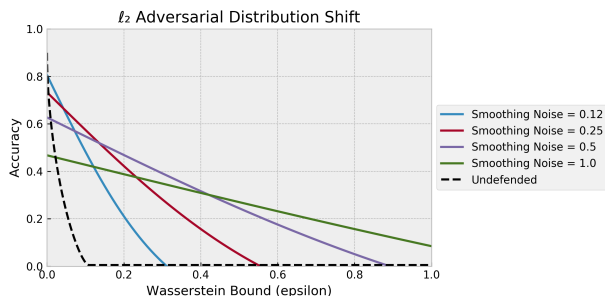


Figure 5. Distributional certificates against ℓ_2 adversarial attacks.

define $\tilde{\mathcal{D}}$ such that $\text{Adv}(x) \sim \tilde{\mathcal{D}}$. It is easy to show that:

$$W_1^d(\mathcal{D}, \tilde{\mathcal{D}}) \leq \mathbb{E}_{x \sim \mathcal{D}}[\|\text{Adv}(x) - x\|_2] \quad (6)$$

So, if the *average* magnitude of perturbations induced by Adv is less than ϵ (i.e., $\mathbb{E}[\|\text{Adv}(x) - x\|_2] < \epsilon$), then $W_1^d(\mathcal{D}, \tilde{\mathcal{D}}) < \epsilon$ and therefore we may apply Theorem 4.1: the gap in the expected accuracy between $x \sim \mathcal{D}$ and $\text{Adv}(x) \sim \tilde{\mathcal{D}}$ will be at most $\psi(\epsilon)$. Note that in this threat model, Adv can be strategic in its use of the average perturbation “budget”: if a certain point x would require a very large perturbation to cause misclassification, or is already misclassified, then $\text{Adv}(x)$ can simply return x , “saving” perturbation budget to successfully attack a greater number of more vulnerable samples.

Note that our method differs from *sample-wise* certificates against ℓ_2 adversarial attacks which use randomized smoothing, such as (Cohen et al., 2019). Specifically, we use only one smoothing perturbation (and therefore only one forward pass) per sample. Our guarantees are on the overall accuracy of the classifier, not on the stability of any particular prediction. Finally, as discussed, our threat model is different, because we allow the adversary to strategically choose which samples to attack, with the certificate dependent on the *Wasserstein* magnitude of the *distributional* attack.

Results on CIFAR-10 are presented in Figure 5. We use ResNet-110 models trained under noise from (Cohen et al., 2019). For the undefended baseline, (on an undefended

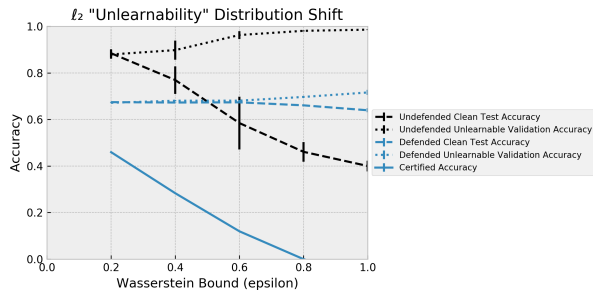


Figure 6. Distributional certificates against unlearnability attacks. Smoothing noise is 0.4; other values are shown in the appendix.

classifier g), we first apply a Carlini and Wagner ℓ_2 attack to each sample x (Carlini & Wagner, 2017), generating adversarial examples x' . Define this attack as the function $CW(\cdot)$, such that $x' = CW(x, y; g)$, where $y = GT(x)$ is the ground-truth label. (If the attack fails, $CW(x, y; g) = x$.) We then define a *strategic* adversary Adv_γ that returns $CW(x, y; g)$ if $\|CW(x, y; g) - x\|_2 < \gamma$, otherwise it returns x . By not attacking samples which would require the largest ℓ_2 perturbations to cause missclassification, this attack efficiently balances maximizing missclassification rate with minimizing the Wasserstein distance between \mathcal{D} and $\tilde{\mathcal{D}}$. The threshold parameter γ controls the tradeoff between missclassification rate and the Wasserstein perturbation magnitude. The ‘Undefended’ baseline in Figure 5 plots the accuracy on attacked test samples under adversary Adv_γ , for a sweep of values of γ , against an upper bound on the Wasserstein distance, given by $\mathbb{E}_{x \sim \mathcal{D}_{test}} [\|\text{Adv}_\gamma(x) - x\|_2]$. (Note that here we are using the finite test distribution \mathcal{D}_{test} , so this is technically an upper bound on $W_1^d(\mathcal{D}_{test}, \tilde{\mathcal{D}}_{test})$.) We can observe a large gap between this undefended model performance under attack, and the certified robustness of our model, showing that our certificate is highly nonvacuous.

7. Hardness Results on Unlearnability

In this section, we show that the pixel-space ℓ_2 -Wasserstein distributional robustness certificate shown above can also be applied to establish a hardness result in creating provably “unlearnable” datasets (Huang et al., 2021). In these datasets, every sample of the released data is “poisoned” so that the accuracy of a classifier trained on this data is high on both the training set and any other (i.e., validation) set split from the released dataset, while the test accuracy on non-poisoned samples drawn from the same distribution is low. This technique has legitimate applications, such as protecting privacy by preventing one’s personal data from being learned, but may also have malicious uses (e.g., a malicious actor could sell a useless classifier that nevertheless has good performance on a provided validation set.) We can view the “clean” data distribution as \mathcal{D} , and the distribution of the poisoned samples (i.e., the unlearnable

distribution) as $\tilde{\mathcal{D}}$. If the magnitude of the perturbations is limited, Theorem 4.1 implies that the accuracy on \mathcal{D} and $\tilde{\mathcal{D}}$ must be similar, implying that our algorithm is provably resistant to unlearnability attacks, effectively establishing provable hardness results to create unlearnable datasets.

In order to apply our guarantees, we must make a few modifications to the attack proposed in (Huang et al., 2021). First, we bound each poisoning perturbation on the released dataset to within an ϵ -radius ℓ_2 ball, rather than an ℓ_∞ ball. From Equation 6, this ensures that $W_1^d(\mathcal{D}, \tilde{\mathcal{D}}) \leq \epsilon$.

Second, we consider an “offline” version of the attack. In the original attack (Huang et al., 2021), perturbations for the entire dataset are optimized simultaneously with a proxy classifier model in an iterative manner. This makes the perturbations applied to each sample non-I.I.D., (because they may depend on each other through proxy-model parameters) which makes deriving generalizable guarantees for it difficult. However, this simultaneous proxy-model training and poisoning may not always represent a realistic threat model. In particular, an actor releasing “unlearnable” data at scale may not be able to constantly update the proxy model being used. For example, consider an “unlearnability” module in a camera, which would make photos unusable as training data. Because the camera itself has access to only a small number of photographs, such a module would likely rely on a fixed, pre-trained proxy classifier model to create the poisoning perturbations. To model this, we consider a threat model where the proxy classifier is first optimized using an unreleased dataset: the released “unlearnable” samples are then perturbed independently using this fixed proxy model. We see in Figure 6 that our modified attack is still highly effective at making data unlearnable, as shown by the high validation and low test accuracy of the undefended baseline.

In Figure 6, we also show the performance of our algorithm on CIFAR-10 under unlearnability attack. We use an “adaptive” attack against the smoothed classifier, inspired by (Salman et al., 2019): details are presented in the appendix. The defense is empirically effective at thwarting unlearnability: the poisoned validation and clean test sets have similar accuracies, even at large perturbation size. However, overall accuracy is reduced substantially. Certified lower bounds on the clean accuracy, computed from the poisoned validation accuracy using Theorem 4.1, are also given.

8. Conclusion

It is possible to certify distributional robustness under natural as well as adversarial shifts in the data distribution. By appropriately parameterizing the transformation space, one can obtain meaningful certificates for natural shifts in data that have a high perturbation size in image space. Our approach could potentially lead to certified robustness techniques for other kinds of shifts such as domain shifts.

9. Acknowledgements

This project was supported in part by NSF CAREER AWARD 1942230, a grant from NIST 60NANB20D134, HR001119S0026 (GARD), ONR grant 13370299 and Army Grant No. W911NF2120076.

References

- Alcorn, M. A., Li, Q., Gong, Z., Wang, C., Mai, L., Ku, W., and Nguyen, A. Strike (with) a pose: Neural networks are easily fooled by strange poses of familiar objects. In *IEEE Conference on Computer Vision and Pattern Recognition, CVPR 2019, Long Beach, CA, USA, June 16-20, 2019*, pp. 4845–4854. Computer Vision Foundation / IEEE, 2019. doi: 10.1109/CVPR.2019.00498.
- Athalye, A., Carlini, N., and Wagner, D. Obfuscated gradients give a false sense of security: Circumventing defenses to adversarial examples. In Dy, J. and Krause, A. (eds.), *Proceedings of the 35th International Conference on Machine Learning*, volume 80 of *Proceedings of Machine Learning Research*, pp. 274–283, Stockholmsmässan, Stockholm Sweden, 10–15 Jul 2018. PMLR.
- Azulay, A. and Weiss, Y. Why do deep convolutional networks generalize so poorly to small image transformations? *Journal of Machine Learning Research*, 20(184):1–25, 2019. URL <http://jmlr.org/papers/v20/19-519.html>.
- Biggio, B., Corona, I., Maiorca, D., Nelson, B., Srndic, N., Laskov, P., Giacinto, G., and Roli, F. Evasion attacks against machine learning at test time. In Blockeel, H., Kersting, K., Nijssen, S., and Zelezný, F. (eds.), *Machine Learning and Knowledge Discovery in Databases - European Conference, ECML PKDD 2013, Prague, Czech Republic, September 23-27, 2013, Proceedings, Part III*, volume 8190 of *Lecture Notes in Computer Science*, pp. 387–402. Springer, 2013. doi: 10.1007/978-3-642-40994-3_25. URL https://doi.org/10.1007/978-3-642-40994-3_25.
- Carlini, N. and Wagner, D. A. Adversarial examples are not easily detected: Bypassing ten detection methods. In *Proceedings of the 10th ACM Workshop on Artificial Intelligence and Security, AISec@CCS 2017, Dallas, TX, USA, November 3, 2017*, pp. 3–14, 2017.
- Clopper, C. J. and Pearson, E. S. The use of confidence or fiducial limits illustrated in the case of the binomial. *Biometrika*, 26(4):404–413, 1934. ISSN 00063444. URL <http://www.jstor.org/stable/2331986>.
- Cohen, J., Rosenfeld, E., and Kolter, Z. Certified adversarial robustness via randomized smoothing. In Chaudhuri, K. and Salakhutdinov, R. (eds.), *Proceedings of the 36th International Conference on Machine Learning*, volume 97 of *Proceedings of Machine Learning Research*, pp. 1310–1320, Long Beach, California, USA, 09–15 Jun 2019. PMLR.
- Courty, N., Flamary, R., Habrard, A., and Rakotomamonjy, A. Joint distribution optimal transportation for domain adaptation. In Guyon, I., von Luxburg, U., Bengio, S., Wallach, H. M., Fergus, R., Vishwanathan, S. V. N., and Garnett, R. (eds.), *Advances in Neural Information Processing Systems 30: Annual Conference on Neural Information Processing Systems 2017, December 4-9, 2017, Long Beach, CA, USA*, pp. 3730–3739, 2017.
- Damodaran, B. B., Kellenberger, B., Flamary, R., Tuia, D., and Courty, N. Deepjdot: Deep joint distribution optimal transport for unsupervised domain adaptation. In Ferrari, V., Hebert, M., Sminchisescu, C., and Weiss, Y. (eds.), *Computer Vision - ECCV 2018 - 15th European Conference, Munich, Germany, September 8-14, 2018, Proceedings, Part IV*, volume 11208 of *Lecture Notes in Computer Science*, pp. 467–483. Springer, 2018. doi: 10.1007/978-3-030-01225-0_28. URL https://doi.org/10.1007/978-3-030-01225-0_28.
- Dodge, S. F. and Karam, L. J. Understanding how image quality affects deep neural networks. *CoRR*, abs/1604.04004, 2016. URL <http://arxiv.org/abs/1604.04004>.
- Engstrom, L., Tran, B., Tsipras, D., Schmidt, L., and Madry, A. Exploring the landscape of spatial robustness. In Chaudhuri, K. and Salakhutdinov, R. (eds.), *Proceedings of the 36th International Conference on Machine Learning, ICML 2019, 9-15 June 2019, Long Beach, California, USA*, volume 97 of *Proceedings of Machine Learning Research*, pp. 1802–1811. PMLR, 2019. URL <http://proceedings.mlr.press/v97/engstrom19a.html>.
- Fawzi, A. and Frossard, P. Manitest: Are classifiers really invariant? *CoRR*, abs/1507.06535, 2015. URL <http://arxiv.org/abs/1507.06535>.
- Fischer, M., Baader, M., and Vechev, M. T. Certified defense to image transformations via randomized smoothing. In Larochelle, H., Ranzato, M., Hadsell, R., Balcan, M., and Lin, H. (eds.), *Advances in Neural Information Processing Systems 33: Annual Conference on Neural Information Processing Systems 2020, NeurIPS 2020, December 6-12, 2020, virtual*, 2020.
- Ge, S., Mishra, S., Wang, H., Li, C., and Jacobs, D. W. Robust contrastive learning using negative samples with diminished semantics. *CoRR*, abs/2110.14189, 2021. URL <https://arxiv.org/abs/2110.14189>.

- Geirhos, R., Temme, C. R. M., Rauber, J., Schütt, H. H., Bethge, M., and Wichmann, F. A. Generalisation in humans and deep neural networks. In Bengio, S., Wallach, H. M., Larochelle, H., Grauman, K., Cesa-Bianchi, N., and Garnett, R. (eds.), *Advances in Neural Information Processing Systems 31: Annual Conference on Neural Information Processing Systems 2018, NeurIPS 2018, December 3-8, 2018, Montréal, Canada*, pp. 7549–7561, 2018.
- Goodfellow, I. J., Shlens, J., and Szegedy, C. Explaining and harnessing adversarial examples. In *3rd International Conference on Learning Representations, ICLR 2015, San Diego, CA, USA, May 7-9, 2015, Conference Track Proceedings*, 2015.
- Gowal, S., Dvijotham, K., Stanforth, R., Bunel, R., Qin, C., Uesato, J., Arandjelovic, R., Mann, T., and Kohli, P. On the effectiveness of interval bound propagation for training verifiably robust models, 2018.
- Hendrycks, D. and Dietterich, T. G. Benchmarking neural network robustness to common corruptions and perturbations. In *7th International Conference on Learning Representations, ICLR 2019, New Orleans, LA, USA, May 6-9, 2019*. OpenReview.net, 2019. URL <https://openreview.net/forum?id=HJz6tiCqYm>.
- Huang, H., Ma, X., Erfani, S. M., Bailey, J., and Wang, Y. Unlearnable examples: Making personal data unexploitable. In *ICLR*, 2021.
- Huang, P., Stanforth, R., Welbl, J., Dyer, C., Yogatama, D., Gowal, S., Dvijotham, K., and Kohli, P. Achieving verified robustness to symbol substitutions via interval bound propagation. In *Proceedings of the 2019 Conference on Empirical Methods in Natural Language Processing and the 9th International Joint Conference on Natural Language Processing, EMNLP-IJCNLP 2019, Hong Kong, China, November 3-7, 2019*, pp. 4081–4091, 2019. doi: 10.18653/v1/D19-1419. URL <https://doi.org/10.18653/v1/D19-1419>.
- Kim, M., Tack, J., and Hwang, S. J. Adversarial self-supervised contrastive learning. In Larochelle, H., Ranzato, M., Hadsell, R., Balcan, M., and Lin, H. (eds.), *Advances in Neural Information Processing Systems 33: Annual Conference on Neural Information Processing Systems 2020, NeurIPS 2020, December 6-12, 2020, virtual*, 2020.
- Kumar, A. and Goldstein, T. Center smoothing: Certified robustness for networks with structured outputs. *Advances in Neural Information Processing Systems*, 34, 2021.
- Kumar, A., Levine, A., and Feizi, S. Policy smoothing for provably robust reinforcement learning. *CoRR*, abs/2106.11420, 2021. URL <https://arxiv.org/abs/2106.11420>.
- Laidlaw, C. and Feizi, S. Functional adversarial attacks. In Wallach, H. M., Larochelle, H., Beygelzimer, A., d’Alché-Buc, F., Fox, E. B., and Garnett, R. (eds.), *Advances in Neural Information Processing Systems 32: Annual Conference on Neural Information Processing Systems 2019, NeurIPS 2019, 8-14 December 2019, Vancouver, BC, Canada*, pp. 10408–10418, 2019. URL <http://papers.nips.cc/paper/9228-functional-adversarial-attacks>.
- Laidlaw, C., Singla, S., and Feizi, S. Perceptual adversarial robustness: Defense against unseen threat models. In *9th International Conference on Learning Representations, ICLR 2021, Virtual Event, Austria, May 3-7, 2021*. OpenReview.net, 2021. URL <https://openreview.net/forum?id=dFwBosAcJkN>.
- Lécuyer, M., Atlidakis, V., Geambasu, R., Hsu, D., and Jana, S. Certified robustness to adversarial examples with differential privacy. In *2019 IEEE Symposium on Security and Privacy, SP 2019, San Francisco, CA, USA, May 19-23, 2019*, pp. 656–672, 2019.
- Lee, J. and Raginsky, M. Minimax statistical learning with wasserstein distances. In Bengio, S., Wallach, H. M., Larochelle, H., Grauman, K., Cesa-Bianchi, N., and Garnett, R. (eds.), *Advances in Neural Information Processing Systems 31: Annual Conference on Neural Information Processing Systems 2018, NeurIPS 2018, December 3-8, 2018, Montréal, Canada*, pp. 2692–2701, 2018.
- Levine, A. and Feizi, S. Wasserstein smoothing: Certified robustness against wasserstein adversarial attacks, 2019.
- Levine, A. and Feizi, S. (de)randomized smoothing for certifiable defense against patch attacks. In Larochelle, H., Ranzato, M., Hadsell, R., Balcan, M., and Lin, H. (eds.), *Advances in Neural Information Processing Systems 33: Annual Conference on Neural Information Processing Systems 2020, NeurIPS 2020, December 6-12, 2020, virtual*, 2020a.
- Levine, A. and Feizi, S. Robustness certificates for sparse adversarial attacks by randomized ablation. In *The Thirty-Fourth AAAI Conference on Artificial Intelligence, AAAI 2020, The Thirty-Second Innovative Applications of Artificial Intelligence Conference, IAAI 2020, The Tenth AAAI Symposium on Educational Advances in Artificial Intelligence, EAAI 2020, New York, NY, USA, February 7-12, 2020*, pp. 4585–4593. AAAI Press, 2020b. URL <https://aaai.org/ojs/index.php/AAAI/article/view/5888>.

- Levine, A. and Feizi, S. Improved, deterministic smoothing for L1 certified robustness. *CoRR*, abs/2103.10834, 2021. URL <https://arxiv.org/abs/2103.10834>.
- Li, B., Chen, C., Wang, W., and Carin, L. Certified adversarial robustness with additive noise. In *Advances in Neural Information Processing Systems 32: Annual Conference on Neural Information Processing Systems 2019, NeurIPS 2019, 8-14 December 2019, Vancouver, BC, Canada*, pp. 9459–9469, 2019.
- Madry, A., Makelov, A., Schmidt, L., Tsipras, D., and Vladu, A. Towards deep learning models resistant to adversarial attacks. In *6th International Conference on Learning Representations, ICLR 2018, Vancouver, BC, Canada, April 30 - May 3, 2018, Conference Track Proceedings*, 2018.
- Maini, P., Wong, E., and Kolter, J. Z. Adversarial robustness against the union of multiple perturbation models. In *Proceedings of the 37th International Conference on Machine Learning, ICML 2020, 13-18 July 2020, Virtual Event*, volume 119 of *Proceedings of Machine Learning Research*, pp. 6640–6650. PMLR, 2020. URL <http://proceedings.mlr.press/v119/maini20a.html>.
- Nicolae, M.-I., Sinn, M., Tran, M. N., Buesser, B., Rawat, A., Wistuba, M., Zantedeschi, V., Baracaldo, N., Chen, B., Ludwig, H., Molloy, I., and Edwards, B. Adversarial robustness toolbox v1.2.0. *CoRR*, 1807.01069, 2018. URL <https://arxiv.org/pdf/1807.01069>.
- Pearce, D. J. B. and Hirsch, H.-G. The aurora experimental framework for the performance evaluation of speech recognition systems under noisy conditions. In *INTER-SPEECH*, 2000.
- Pinot, R., Meunier, L., Yger, F., Gouy-Pailler, C., Chevalleyre, Y., and Atif, J. On the robustness of randomized classifiers to adversarial examples. *CoRR*, abs/2102.10875, 2021. URL <https://arxiv.org/abs/2102.10875>.
- Radford, A., Kim, J. W., Hallacy, C., Ramesh, A., Goh, G., Agarwal, S., Sastry, G., Askell, A., Mishkin, P., Clark, J., Krueger, G., and Sutskever, I. Learning transferable visual models from natural language supervision. In Meila, M. and Zhang, T. (eds.), *Proceedings of the 38th International Conference on Machine Learning, ICML 2021, 18-24 July 2021, Virtual Event*, volume 139 of *Proceedings of Machine Learning Research*, pp. 8748–8763. PMLR, 2021. URL <http://proceedings.mlr.press/v139/radford21a.html>.
- Raghunathan, A., Steinhardt, J., and Liang, P. Semidefinite relaxations for certifying robustness to adversarial examples. In *Proceedings of the 32nd International Conference on Neural Information Processing Systems, NIPS’18*, pp. 10900–10910, Red Hook, NY, USA, 2018. Curran Associates Inc.
- Salman, H., Li, J., Razenshteyn, I. P., Zhang, P., Zhang, H., Bubeck, S., and Yang, G. Provably robust deep learning via adversarially trained smoothed classifiers. In *Advances in Neural Information Processing Systems 32: Annual Conference on Neural Information Processing Systems 2019, NeurIPS 2019, 8-14 December 2019, Vancouver, BC, Canada*, pp. 11289–11300, 2019.
- Shafahi, A., Najibi, M., Ghiasi, A., Xu, Z., Dickerson, J. P., Studer, C., Davis, L. S., Taylor, G., and Goldstein, T. Adversarial training for free! In Wallach, H. M., Larochelle, H., Beygelzimer, A., d’Alché-Buc, F., Fox, E. B., and Garnett, R. (eds.), *Advances in Neural Information Processing Systems 32: Annual Conference on Neural Information Processing Systems 2019, NeurIPS 2019, December 8-14, 2019, Vancouver, BC, Canada*, pp. 3353–3364, 2019.
- Singla, S. and Feizi, S. Robustness certificates against adversarial examples for relu networks. *CoRR*, abs/1902.01235, 2019.
- Singla, S. and Feizi, S. Second-order provable defenses against adversarial attacks. In *Proceedings of the 37th International Conference on Machine Learning, ICML 2020, 13-18 July 2020, Virtual Event*, volume 119 of *Proceedings of Machine Learning Research*, pp. 8981–8991. PMLR, 2020. URL <http://proceedings.mlr.press/v119/singla20a.html>.
- Sinha, A., Namkoong, H., and Duchi, J. C. Certifying some distributional robustness with principled adversarial training. In *6th International Conference on Learning Representations, ICLR 2018, Vancouver, BC, Canada, April 30 - May 3, 2018, Conference Track Proceedings*. OpenReview.net, 2018. URL <https://openreview.net/forum?id=Hk6kPgZA->.
- Szegedy, C., Zaremba, W., Sutskever, I., Bruna, J., Erhan, D., Goodfellow, I. J., and Fergus, R. Intriguing properties of neural networks. In *2nd International Conference on Learning Representations, ICLR 2014, Banff, AB, Canada, April 14-16, 2014, Conference Track Proceedings*, 2014.
- Taori, R., Dave, A., Shankar, V., Carlini, N., Recht, B., and Schmidt, L. Measuring robustness to natural distribution shifts in image classification. In Larochelle, H., Ranzato, M., Hadsell, R., Balcan, M., and Lin, H. (eds.), *Advances in Neural Information Processing Systems 33: Annual Conference on Neural Information Processing Systems 2020, NeurIPS 2020, December 6-12, 2020, virtual*, 2020.

- Tramèr, F. and Boneh, D. Adversarial training and robustness for multiple perturbations. In Wallach, H. M., Larochelle, H., Beygelzimer, A., d'Alché-Buc, F., Fox, E. B., and Garnett, R. (eds.), *Advances in Neural Information Processing Systems 32: Annual Conference on Neural Information Processing Systems 2019, NeurIPS 2019, December 8-14, 2019, Vancouver, BC, Canada*, pp. 5858–5868, 2019.
- Uesato, J., O’Donoghue, B., Kohli, P., and van den Oord, A. Adversarial risk and the dangers of evaluating against weak attacks. In *Proceedings of the 35th International Conference on Machine Learning, ICML 2018, Stockholmsmässan, Stockholm, Sweden, July 10-15, 2018*, pp. 5032–5041, 2018.
- Vasiljevic, I., Chakrabarti, A., and Shakhnarovich, G. Examining the impact of blur on recognition by convolutional networks. *CoRR*, abs/1611.05760, 2016. URL <http://arxiv.org/abs/1611.05760>.
- Wong, E. and Kolter, J. Z. Provable defenses against adversarial examples via the convex outer adversarial polytope. In *Proceedings of the 35th International Conference on Machine Learning, ICML 2018, Stockholmsmässan, Stockholm, Sweden, July 10-15, 2018*, pp. 5283–5292, 2018.
- Wong, E., Schmidt, F. R., and Kolter, J. Z. Wasserstein adversarial examples via projected sinkhorn iterations. In Chaudhuri, K. and Salakhutdinov, R. (eds.), *Proceedings of the 36th International Conference on Machine Learning, ICML 2019, 9-15 June 2019, Long Beach, California, USA*, volume 97 of *Proceedings of Machine Learning Research*, pp. 6808–6817. PMLR, 2019. URL <http://proceedings.mlr.press/v97/wong19a.html>.
- Wu, F., Li, L., Huang, Z., Vorobeychik, Y., Zhao, D., and Li, B. CROP: certifying robust policies for reinforcement learning through functional smoothing. *CoRR*, abs/2106.09292, 2021. URL <https://arxiv.org/abs/2106.09292>.
- Wu, Y., Winston, E., Kaushik, D., and Lipton, Z. C. Domain adaptation with asymmetrically-relaxed distribution alignment. In Chaudhuri, K. and Salakhutdinov, R. (eds.), *Proceedings of the 36th International Conference on Machine Learning, ICML 2019, 9-15 June 2019, Long Beach, California, USA*, volume 97 of *Proceedings of Machine Learning Research*, pp. 6872–6881. PMLR, 2019. URL <http://proceedings.mlr.press/v97/wu19f.html>.
- Yang, F., Wang, Z., and Heinze-Deml, C. Invariance-inducing regularization using worst-case transformations suffices to boost accuracy and spatial robustness. In Wallach, H. M., Larochelle, H., Beygelzimer, A., d’Alché-Buc, F., Fox, E. B., and Garnett, R. (eds.), *Advances in Neural Information Processing Systems 32: Annual Conference on Neural Information Processing Systems 2019, NeurIPS 2019, December 8-14, 2019, Vancouver, BC, Canada*, pp. 14757–14768, 2019.
- Zhou, Y., Song, S., and Cheung, N. On classification of distorted images with deep convolutional neural networks. *CoRR*, abs/1701.01924, 2017. URL <http://arxiv.org/abs/1701.01924>.

A. Proof of Lemma 3.1

Statement. For two points $x, z \in \mathcal{X}$ such that $d_{\mathcal{T}}(x, z)$ is finite,

$$\text{TV}(\mathcal{S}(x), \mathcal{S}(z)) \leq \psi(d_{\mathcal{T}}(x, z)).$$

Proof. Consider the θ for which $d_{\mathcal{T}}(x, z) = \|\theta\|$. Then, $\mathcal{T}(x, \theta) = z$.

$$\begin{aligned} \text{TV}(\mathcal{S}(x), \mathcal{S}(z)) &= \text{TV}(\mathcal{T}(x, \mathcal{Q}(0)), \mathcal{T}(z, \mathcal{Q}(0))) \\ &= \text{TV}(\mathcal{T}(x, \mathcal{Q}(0)), \mathcal{T}(\mathcal{T}(x, \theta), \mathcal{Q}(0))) \\ &= \text{TV}(\mathcal{T}(x, \mathcal{Q}(0)), \mathcal{T}(x, \theta + \mathcal{Q}(0))) && \text{(additive composability, equation (4))} \\ &= \text{TV}(\mathcal{T}(x, \mathcal{Q}(0)), \mathcal{T}(x, \mathcal{Q}(\theta))). && \text{(definition of } \mathcal{Q}) \end{aligned}$$

Let A be the event in the space M that maximizes the difference in the probabilities assigned to A by $\mathcal{T}(x, \mathcal{Q}(0))$ and $\mathcal{T}(x, \mathcal{Q}(\theta))$. Let $u : P \rightarrow [0, 1]$ be a function that returns the probability (over the randomness of \mathcal{T}) of any parameter $\eta \in P$ being mapped to a point in A , i.e., $u(\eta) = \mathbb{P}\{\mathcal{T}(x, \eta) \in A\}$. For a deterministic transformation \mathcal{T} , u is a 0/1 function. Then, the probabilities assigned by $\mathcal{T}(x, \mathcal{Q}(0))$ and $\mathcal{T}(x, \mathcal{Q}(\theta))$ to A is equal to $\mathbb{E}_{\eta \sim \mathcal{Q}(0)}[u(\eta)]$ and $\mathbb{E}_{\eta \sim \mathcal{Q}(\theta)}[u(\eta)]$. Therefore,

$$\begin{aligned} \text{TV}(\mathcal{S}(x), \mathcal{S}(z)) &= |\mathbb{E}_{\eta \sim \mathcal{Q}(0)}[u(\eta)] - \mathbb{E}_{\eta \sim \mathcal{Q}(\theta)}[u(\eta)]| \\ &\leq \text{TV}(\mathcal{Q}(0), \mathcal{Q}(\theta)) \\ &\leq \psi(\|\theta\|) = \psi(d_{\mathcal{T}}(x, z)). && \text{(definition of } \mathcal{Q} \text{ and } d_{\mathcal{T}}) \end{aligned}$$

□

B. Function ψ for Different Distributions

For an isometric Gaussian distribution $\mathcal{N}(0, \sigma^2 I)$,

$$\text{TV}(\mathcal{N}(0, \sigma^2 I), \mathcal{N}(\theta, \sigma^2 I)) = \text{erf}(\|\theta\|_2 / 2\sqrt{2}\sigma).$$

Proof. Due to the isometric symmetry of the Gaussian distribution and the ℓ_2 -norm, we may assume, without loss of generality, that $\mathcal{N}(\theta, \sigma^2 I)$ is obtained by shifting $\mathcal{N}(0, \sigma^2 I)$ only along the first dimension. Therefore, the total variation of the two distributions is equal to the difference in the probability of a normal random variable with variance σ^2 being less than $\|\theta\|_2/2$ and $-\|\theta\|_2/2$, i.e., $\Phi(\|\theta\|_2/2\sigma) - \Phi(-\|\theta\|_2/2\sigma)$ where Φ is the standard normal CDF.

$$\begin{aligned} \text{TV}(\mathcal{N}(0, \sigma^2 I), \mathcal{N}(\theta, \sigma^2 I)) &= \Phi(\|\theta\|_2/2\sigma) - \Phi(-\|\theta\|_2/2\sigma) \\ &= 2\Phi(\|\theta\|_2/2\sigma) - 1 \\ &= 2 \left(\frac{1 + \text{erf}(\|\theta\|_2/2\sqrt{2}\sigma)}{2} \right) - 1 \\ &= \text{erf}(\|\theta\|_2/2\sqrt{2}\sigma). \end{aligned}$$

□

For a uniform distribution $\mathcal{U}(\theta, b)$ between θ_i and $\theta_i + b$ in each dimension for $b \geq 0$ (as used for the SV shift transformations), $\text{TV}(\mathcal{U}(0, b), \mathcal{U}(\theta, b)) \leq \|\theta\|_1/b$. When $\|\theta\|_1$ is constrained, the volume of the overlap between $\mathcal{U}(0, b)$ and $\mathcal{U}(\theta, b)$ is minimized when the shift is only along one dimension.

C. Proof of Theorem 5.1

Statement. The transformation CS satisfies the additive composability property, i.e., $\forall x \in M, \theta_1, \theta_2 \in \mathbb{R}^3$,

$$\text{CS}(\text{CS}(x, \theta_1), \theta_2) = \text{CS}(x, \theta_1 + \theta_2).$$

Proof. Let $x = \{(r, g, b)_{ij}\}^{H \times W}$, $x' = \{(r', g', b')_{ij}\}^{H \times W} = \text{CS}(x, \theta_1)$ and $x'' = \{(r'', g'', b'')_{ij}\}^{H \times W} = \text{CS}(x', \theta_2)$. We need to show that $x'' = \text{CS}(x, \theta_1 + \theta_2)$. Let r_{\max}, g_{\max} and b_{\max} be the maximum values of the red, green and blue channels respectively of x and r'_{\max}, g'_{\max} and b'_{\max} be the same for x' . From the definition of CS in section 5.1, we have:

$$\begin{aligned} r'_{ij} &= \frac{2^{\theta_1^R} r_{ij}}{\text{MAX}}, & g'_{ij} &= \frac{2^{\theta_1^G} g_{ij}}{\text{MAX}}, & b'_{ij} &= \frac{2^{\theta_1^B} b_{ij}}{\text{MAX}} \\ \text{and } r''_{ij} &= \frac{2^{\theta_2^R} r'_{ij}}{\text{MAX}'}, & g''_{ij} &= \frac{2^{\theta_2^G} g'_{ij}}{\text{MAX}'}, & b''_{ij} &= \frac{2^{\theta_2^B} b'_{ij}}{\text{MAX}'} \end{aligned}$$

where $\text{MAX} = \max(2^{\theta_1^R} r_{\max}, 2^{\theta_1^G} g_{\max}, 2^{\theta_1^B} b_{\max})$ and $\text{MAX}' = \max(2^{\theta_2^R} r'_{\max}, 2^{\theta_2^G} g'_{\max}, 2^{\theta_2^B} b'_{\max})$. From the definition of r'_{\max} , we have:

$$r'_{\max} = \max r'_{ij} = \max \frac{2^{\theta_1^R} r_{ij}}{\text{MAX}} = \frac{2^{\theta_1^R} \max r_{ij}}{\text{MAX}} = \frac{2^{\theta_1^R} r_{\max}}{\text{MAX}}.$$

Similarly,

$$g'_{\max} = \frac{2^{\theta_1^G} g_{\max}}{\text{MAX}} \quad \text{and} \quad b'_{\max} = \frac{2^{\theta_1^B} b_{\max}}{\text{MAX}}.$$

Therefore,

$$\text{MAX}' = \frac{\max(2^{\theta_1^R + \theta_2^R} r_{\max}, 2^{\theta_1^G + \theta_2^G} g_{\max}, 2^{\theta_1^B + \theta_2^B} b_{\max})}{\text{MAX}}.$$

Substituting r'_{ij} and MAX' in the expression for r''_{ij} , we get:

$$r''_{ij} = \frac{2^{\theta_2^R} 2^{\theta_1^R} r_{ij}}{\text{MAX}' \text{MAX}} = \frac{2^{\theta_1^R + \theta_2^R} r_{ij}}{\max(2^{\theta_1^R + \theta_2^R} r_{\max}, 2^{\theta_1^G + \theta_2^G} g_{\max}, 2^{\theta_1^B + \theta_2^B} b_{\max})}.$$

Similarly,

$$g''_{ij} = \frac{2^{\theta_1^G + \theta_2^G} g_{ij}}{\max(2^{\theta_1^R + \theta_2^R} r_{\max}, 2^{\theta_1^G + \theta_2^G} g_{\max}, 2^{\theta_1^B + \theta_2^B} b_{\max})} \quad \text{and} \quad b''_{ij} = \frac{2^{\theta_1^B + \theta_2^B} b_{ij}}{\max(2^{\theta_1^R + \theta_2^R} r_{\max}, 2^{\theta_1^G + \theta_2^G} g_{\max}, 2^{\theta_1^B + \theta_2^B} b_{\max})}.$$

Hence, $x'' = \text{CS}(x, \theta_1 + \theta_2)$. \square

D. Proof of Theorem 5.2

Statement. The transformation SV satisfies the additive composability property, i.e., $\forall x \in M, \theta_1, \theta_2 \in \mathbb{R}_{\geq 0}^2$,

$$\text{SV}(\text{SV}(x, \theta_1), \theta_2) = \text{SV}(x, \theta_1 + \theta_2).$$

Proof. Let $x = \{(h, s, v)_{ij}\}^{H \times W}$, $x' = \{(h, s', v')_{ij}\}^{H \times W} = \text{SV}(x, \theta_1)$ and $x'' = \{(h, s'', v'')_{ij}\}^{H \times W} = \text{SV}(x', \theta_2)$ in HSV format. We need to show that $x'' = \text{SV}(x, \theta_1 + \theta_2)$. Let $s_{\text{mean}}, s_{\max}, v_{\text{mean}}$ and v_{\max} be the means and maximums of the saturation and brightness values of x and $s'_{\text{mean}}, s'_{\max}, v'_{\text{mean}}$ and v'_{\max} be the same for x' . From the definition of SV in section 5.3, we have:

$$\begin{aligned} s'_{ij} &= \frac{s_{ij} + (2^{\theta_1^S} - 1)s_{\text{mean}}}{\text{MAX}}, & v'_{ij} &= \frac{v_{ij} + (2^{\theta_1^V} - 1)v_{\text{mean}}}{\text{MAX}} \\ \text{and } s''_{ij} &= \frac{s'_{ij} + (2^{\theta_2^S} - 1)s'_{\text{mean}}}{\text{MAX}'}, & v''_{ij} &= \frac{v'_{ij} + (2^{\theta_2^V} - 1)v'_{\text{mean}}}{\text{MAX}'} \end{aligned}$$

where $\text{MAX} = \max(s_{\max} + (2^{\theta_1^S} - 1)s_{\text{mean}}, v_{\max} + (2^{\theta_1^V} - 1)v_{\text{mean}})$ and $\text{MAX}' = \max(s'_{\max} + (2^{\theta_2^S} - 1)s'_{\text{mean}}, v'_{\max} + (2^{\theta_2^V} - 1)v'_{\text{mean}})$. From the definitions of s'_{mean} and s'_{\max} , we have:

$$\begin{aligned} s'_{\text{mean}} &= \text{mean } s'_{ij} = \text{mean } \frac{s_{ij} + (2^{\theta_1^S} - 1)s_{\text{mean}}}{\text{MAX}} = \frac{\text{mean } s_{ij} + (2^{\theta_1^S} - 1)s_{\text{mean}}}{\text{MAX}} = \frac{2^{\theta_1^S} s_{\text{mean}}}{\text{MAX}} \\ s'_{\max} &= \max s'_{ij} = \max \frac{s_{ij} + (2^{\theta_1^S} - 1)s_{\text{mean}}}{\text{MAX}} = \frac{\max s_{ij} + (2^{\theta_1^S} - 1)s_{\text{mean}}}{\text{MAX}} = \frac{s_{\max} + (2^{\theta_1^S} - 1)s_{\text{mean}}}{\text{MAX}}. \end{aligned}$$

Similarly,

$$v'_{\text{mean}} = \frac{2^{\theta_1^V} v_{\text{mean}}}{\text{MAX}} \quad \text{and} \quad v'_{\text{max}} = \frac{v_{\text{max}} + (2^{\theta_1^V} - 1)v_{\text{mean}}}{\text{MAX}}.$$

Therefore,

$$\begin{aligned} \text{MAX}' &= \max(s'_{\text{max}} + (2^{\theta_2^S} - 1)s'_{\text{mean}}, v'_{\text{max}} + (2^{\theta_2^V} - 1)v'_{\text{mean}}) \\ &= \max\left(\frac{s_{\text{max}} + (2^{\theta_1^S} - 1)s_{\text{mean}} + (2^{\theta_2^S} - 1)2^{\theta_1^S} s_{\text{mean}}}{\text{MAX}}, v'_{\text{max}} + (2^{\theta_2^V} - 1)v'_{\text{mean}}\right) \\ &= \max\left(\frac{s_{\text{max}} + (2^{\theta_1^S + \theta_2^S} - 1)s_{\text{mean}}}{\text{MAX}}, v'_{\text{max}} + (2^{\theta_2^V} - 1)v'_{\text{mean}}\right) \\ &= \max(s_{\text{max}} + (2^{\theta_1^S + \theta_2^S} - 1)s_{\text{mean}}, v_{\text{max}} + (2^{\theta_1^V} - 1)v_{\text{mean}} + (2^{\theta_2^V} - 1)2^{\theta_1^V} v_{\text{mean}})/\text{MAX} \\ &= \max(s_{\text{max}} + (2^{\theta_1^S + \theta_2^S} - 1)s_{\text{mean}}, v_{\text{max}} + (2^{\theta_1^V + \theta_2^V} - 1)v_{\text{mean}})/\text{MAX}. \end{aligned}$$

Substituting s'_{ij} , s'_{mean} and MAX' in the expression for s''_{ij} , we get:

$$\begin{aligned} s''_{ij} &= \frac{s_{ij} + (2^{\theta_1^S} - 1)s_{\text{mean}} + (2^{\theta_2^S} - 1)2^{\theta_1^S} s_{\text{mean}}}{\text{MAX}'\text{MAX}} \\ &= \frac{s_{ij} + (2^{\theta_1^S + \theta_2^S} - 1)s_{\text{mean}}}{\max(s_{\text{max}} + (2^{\theta_1^S + \theta_2^S} - 1)s_{\text{mean}}, v_{\text{max}} + (2^{\theta_1^V + \theta_2^V} - 1)v_{\text{mean}})}. \end{aligned}$$

Similarly,

$$v''_{ij} = \frac{v_{ij} + (2^{\theta_1^V + \theta_2^V} - 1)v_{\text{mean}}}{\max(s_{\text{max}} + (2^{\theta_1^S + \theta_2^S} - 1)s_{\text{mean}}, v_{\text{max}} + (2^{\theta_1^V + \theta_2^V} - 1)v_{\text{mean}})}.$$

Hence, $x'' = \text{SV}(x, \theta_1 + \theta_2)$. □

E. Details for Plots in Figure 2

The distribution shifts used to evaluate the empirical performance of the base models in figure 2 have been generated by first sampling an image x from the original distribution \mathcal{D} and then randomly transforming it images from the original distribution by adding a noise in the corresponding transformation space. The Wasserstein bound of these shifts can be calculated by computing the expected perturbation size of the smoothing distribution. For example, the expected ℓ_2 -norm of a 3-dimensional Gaussian vector is given by $2\sqrt{2}\sigma/\sqrt{\pi}$ and expected ℓ_1 -norm a 2-dimensional vector sampled uniformly from $[0, b]^2$ is b .

The training and smoothing noise levels used for color shift, hue shift and SV shift are (0.8, 10.0), (180°, 180°) and (8.0, 12.0) respectively.

F. Hue Shift Plot

In figure 7, we plot the certified accuracies obtained by various models trained using different noise levels, i.e., random hue rotations picked uniformly from the range $[-\beta, \beta]$ for different values of the maximum angle β in the range. The certified accuracy roughly increases with the training noise achieving a maximum of 87.9% for a max angle $\beta = 180^\circ$ for the training noise level.

G. Random Channel Selection

Consider a smoothing distribution that randomly picks one of the RGB channels with equal probability, scales it so that the maximum pixel value in that channel is one and sets all the other channels to zero. This smoothing distribution is invariant to the color shift transformation CS and thus, satisfies $\psi(d_{\mathcal{T}}(x, z)) = 0$ whenever $d_{\mathcal{T}}(x, z)$ is finite. Therefore, from theorem 4.1, we have $\mathbb{E}_{z \sim \bar{\mathcal{D}}}[\bar{h}(z)] \geq \mathbb{E}_{x \sim \mathcal{D}}[\bar{h}(x)]$ under this smoothing distribution for all Wasserstein bounds ϵ with respect to d_{CS} . Figure 8 plots the certified accuracies, using random channel selection for smoothing, achieved by models trained using Gaussian distributions of varying noise levels in the transformation space. The certified accuracy roughly increases with the training noise achieving a maximum of 87.1% for a training noise of 0.8.

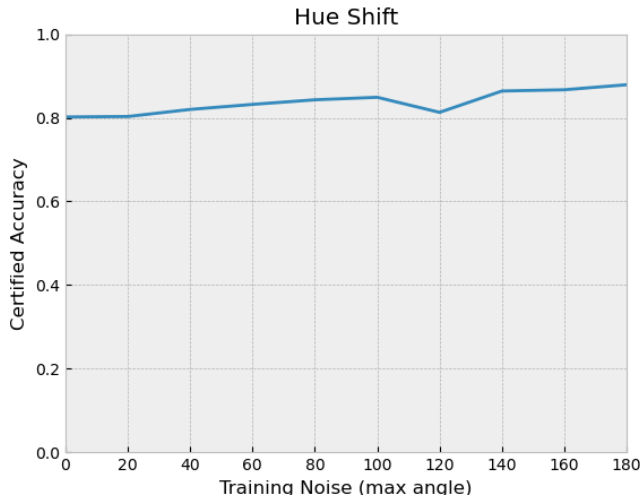


Figure 7. Certified accuracy under hue shift for different levels of training noise. Since, the certified accuracy remains constant with respect to the Wasserstein distance (ϵ) of the shifted distribution, we plot the certified accuracy of models trained with different noise levels β .

H. Experiment Details for Section 6

As mentioned, for the certified models, we use the released pre-trained ResNet110 models from (Cohen et al., 2019), using the same level of Gaussian Noise for training and testing. For empirical results, we use the implementation of the ℓ_2 Carlini and Wagner (Carlini & Wagner, 2017) attack provided by the IBM ART package (Nicolae et al., 2018) with default parameters (except for batch size which we set at 256 to increase processing speed.)

I. Experiment details for Section 7

Our experimental setting is adapted from the “sample-wise perturbation” CIFAR-10 experiments in (Huang et al., 2021): hyperparameters are the same as in that work unless otherwise stated. For background, (Huang et al., 2021) creates an unlearnable dataset by performing the following “bi-level” minimization, to simultaneously train a proxy classifier model and create unlearnable examples:

$$\min_{\theta} \min_{(\epsilon_1, \dots, \epsilon_n)} \frac{1}{n} \sum_{i=1}^n \mathcal{L}(f_{\theta}(x_i + \epsilon_i), y_i) \quad (7)$$

In other words, in contrast with standard training, both the samples and the proxy classifier are optimized to decrease the loss. New classifiers trained on the resulting samples fail to generalize to unperturbed samples. In the experiments, as in (Huang et al., 2021), the inner minimization over perturbations is performed for 20 steps over the entire dataset, for every one batch update step of the outer minimization. Training stops when training accuracy reaches a threshold value of 99%.

We now detail differences in experimental setup from (Huang et al., 2021):

I.1. Adaptation to ℓ_2 attack setting

After each optimization step, we project ϵ_i ’s into an ℓ_2 ball (of radius given by the Wasserstein bound ϵ) rather than an ℓ_{∞} ball. We also use an ℓ_2 PGD step:

$$\epsilon'_i = \epsilon_i + \tau \frac{\nabla_{\epsilon_i} \mathcal{L}(\cdot)}{\|\nabla_{\epsilon_i} \mathcal{L}(\cdot)\|_2} \quad (8)$$

Step size τ was set as 0.1 times the total ℓ_2 ϵ bound.

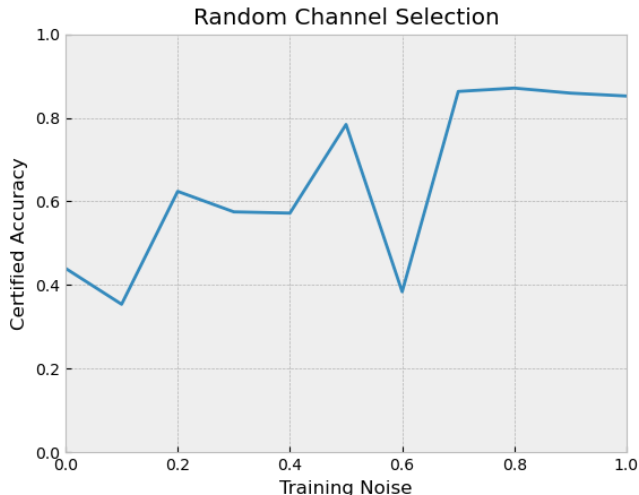


Figure 8. Certified robustness against color shift using random channel selection as the smoothing distribution. Since, the certified accuracy remains constant with respect to the Wasserstein distance (ϵ) of the shifted distribution, we plot the certified accuracy of models trained with various levels of Gaussian noise in the transformation space.

I.2. Adaptation to offline setting

As discussed in the test, we modify the algorithm such that the simultaneous training of the proxy model and generation of perturbations does not introduce statistical dependencies between perturbed training samples. This is especially important because, if the victim later makes a train-validation split, this would introduce statistical dependencies between training and validation samples, making it hard to generalize certificates to a test set.

To avoid this, we construct four data splits:

- Test set (10000 samples): The original CIFAR-10 test set. Never perturbed, only used in final model evaluation.
- Proxy training set (20000 samples): Used for the optimization of the proxy classifier model parameters θ in Equation 7 and discarded afterward.
- Training set (20000 samples): Perturbed using one round of the the standard 20 steps of the inner optimization of Equation 7, while keeping θ fixed.
- Validation set (10000 samples): Perturbed using the same method as the “Training set.”

The victim model is trained on the “Training Set” and evaluated on the “Validation set” and “Test set”. We also tested on the clean (unperturbed) version of the validation set.

I.3. Adaptive attack setting

When testing our smoothing algorithm, we tested two types of attacks:

- Non-adaptive attack: the proxy model is trained and perturbations are generated using undefended models without smoothing: only the victim policy applies smoothing noise during training and evaluation.
- Adaptive attack: In the minimization of Equation 7, the loss term $\mathcal{L}(f_\theta(x_i + \epsilon_i), y_i)$ is replaced by the expectation:

$$\mathbb{E}_{\delta \sim \mathcal{N}(0, \sigma^2 I)} \mathcal{L}(f_\theta(x_i + \epsilon_i + \delta), y_i) \quad (9)$$

In other words, this models the expectation of a *smoothed* model, like the victim classifier. This smoothed optimization is used in both the proxy model training, as well as the generation of the training and validation sets. Following

(Salman et al., 2019), which proposed a similar adaptive attack for sample-wise smoothed classifiers we approximate the expectation using a small number of random perturbations, which are held fixed for the 20 steps of the inner optimization. In our experiments, we use 8 samples for approximation. Because, at large smoothing noises, this makes the attack much less effective, we cut off training after 20 steps of the outer maximization, rather than relying on the accuracy to reach 99%. (the maximum number of steps required to converge we observed for the non-adaptive attack was 15).

I.4. Results

Complete experimental results are presented in Figure 9. All results are means of 5 independent runs, and error bars represent standard errors of the means.

Certifying Model Accuracy under Distribution Shifts

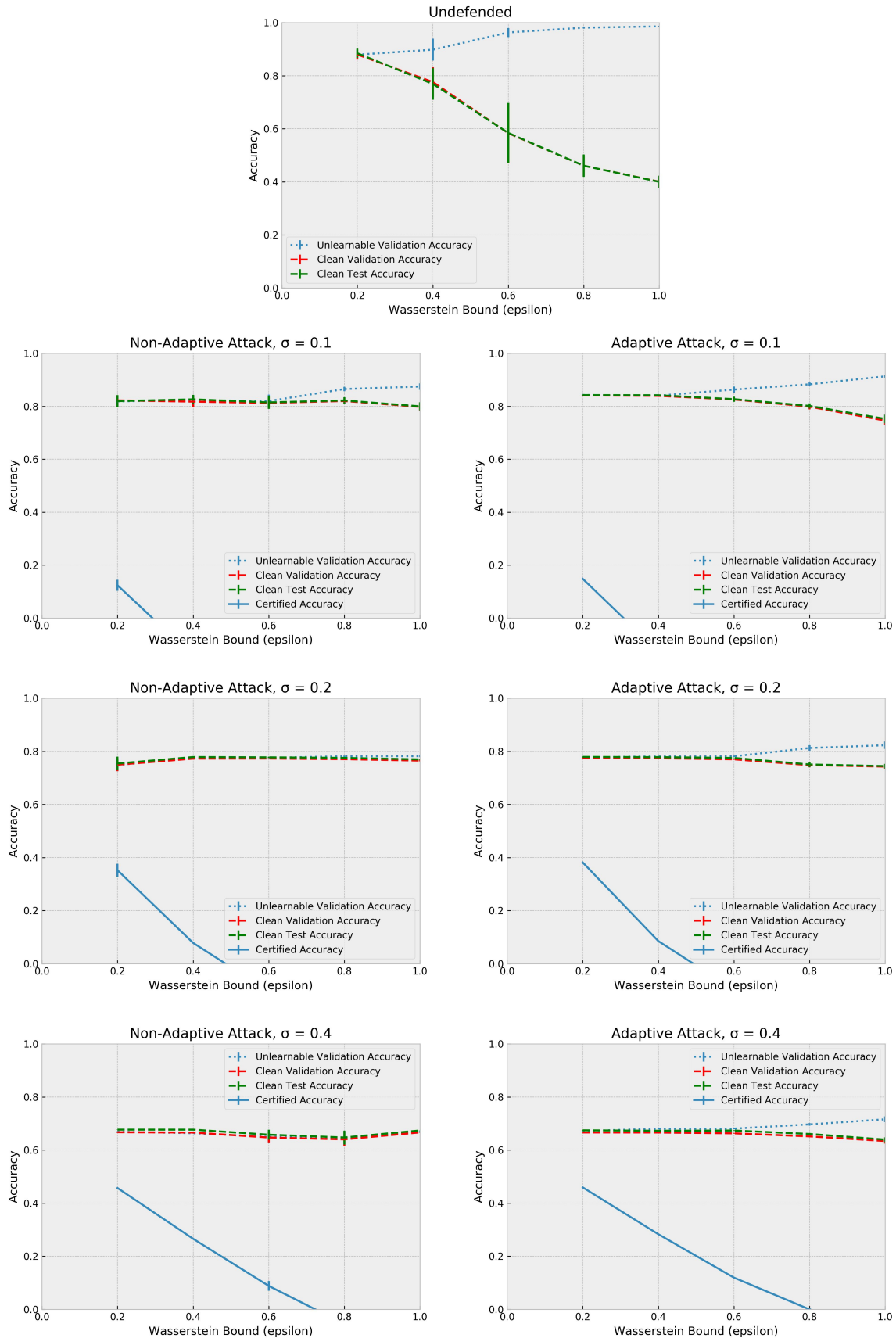


Figure 9. Complete Experimental results for unlearnability experiments.